Available online at www.sciencedirect.com
ScienceDirect
Journal of Computational Physics 227 (2007) 877–885
JOURNAL OF COMPUTATIONAL PHYSICS
www.elsevier.com/locate/jcp

Short Note

On the connection between the spectral volume and the spectral difference method

Kris Van den Abeele [a,*,1], Chris Lacor [a], Z.J. Wang [b]

[a] *Vrije Universiteit Brussel, Department of Mechanical Engineering, Fluid Dynamics and Thermodynamics Research Group, Pleinlaan 2, 1050 Brussels, Belgium*
[b] *Department of Aerospace Engineering, Iowa State University, 2271 Howe Hall, Ames, IA 50011, United States*

Received 11 April 2007; received in revised form 28 August 2007; accepted 30 August 2007
Available online 14 September 2007

Keywords: Spectral volume method; Spectral difference method

1. Introduction

In the last few years, two new high-order accurate methods for unstructured grids have been developed, namely the spectral volume (SV) and the spectral difference (SD) method. Both methods are related to the well-known discontinuous Galerkin (DG) method, see for instance [1], in the sense that they also use piecewise continuous polynomials as solution approximation space. The development of the SV method was mainly reported in publications by Wang [2], Wang et al. [3–5,8], Liu et al. [6] and Sun et al. [7]. Further contributions were made by Chen [12,13], Van den Abeele et al. [14] and Van den Abeele and Lacor [15]. The development of the SD method was reported more recently in publications by Liu et al. [9] and Wang et al. [10]. In 1D, the SD method is identical to the multi-domain spectral method proposed by Kopriva [11].

The SV method is strongly related to the finite volume (FV) method. As with the FV method, the SV solution variables are averaged values over control volumes (CVs) and the residuals corresponding to these solution variables can be written as the sum of the fluxes through the CV faces. The SV method differs from the FV method in the choice of the stencils used to approximate the fluxes through these CV faces. By partitioning each cell, or spectral volume (SV), into CVs in a similar way, a unique stencil, valid for all cells in the mesh, can be obtained. This is the major advantage of the SV method over high-order accurate unstructured FV methods, where these stencils depend on the local mesh geometry. At faces between two SVs, a Riemann solver is used to compute a unique flux from the two solutions in the neighbouring SVs.

Similarly, the SD method is strongly related to the finite difference (FD) method. For both the FD and the SD method, the solution variables are pointwise values, for which the residuals can be written as a function of the flux derivatives in the solution points. With the SD method the computational domain is subdivided in

* Corresponding author. Tel.: +32 26292399; fax: +32 26292880.
E-mail addresses: kvdabeel@vub.ac.be (K. Van den Abeele), chris.lacor@vub.ac.be (C. Lacor), zjw@iastate.edu (Z.J. Wang).
[1] FWO Research Engineer.

0021-9991/$ - see front matter
doi:10.1016/j.jcp.2007.08.030

cells, and in each cell, solution and flux points are placed in a similar way, to arrive at a unique stencil, independent of the local mesh geometry, for the flux derivatives in the solution points. The solutions in the different cells are again coupled through Riemann solvers.

The FV and the FD method are equivalent in 1D for a uniform mesh. In this note, it will be shown that a similar equivalence exists between the SV and the SD methods. The note is further organised as follows. In Sections 2 and 3, the SV and the SD methods for 1D are briefly reviewed. The equivalence between these methods will then be proven in Section 4. In Section 5, this equivalence will be illustrated for the linear advection equation and for Burger's equation in 1D, and finally conclusions will be drawn in Section 6.

2. Spectral volume method in 1D

The 1D SV method is applicable to hyperbolic conservation law systems of the following form:

$$\frac{\partial \mathbf{u}}{\partial t} + \frac{\partial \mathbf{f}(\mathbf{u})}{\partial x} = 0 \tag{1}$$

with $\mathbf{u}$ a column vector containing the conserved variables and $\mathbf{f}(\mathbf{u})$ the fluxes. The computational domain $x_l \leqslant x \leqslant x_r$ over which this conservation law is valid is divided in N cells (SVs) with index $i : x_{i-\frac{1}{2}} \leqslant x \leqslant x_{i+\frac{1}{2}}$, such that $x_{\frac{1}{2}} \equiv x_l$ and $x_{N+\frac{1}{2}} \equiv x_r$. For a $(p+1)$th-order accurate scheme, these cells are then further subdivided into $p+1$ CVs, with index j and boundaries $x^{\mathrm{b}}_{i,j-\frac{1}{2}}$ and $x^{\mathrm{b}}_{i,j+\frac{1}{2}}$. In Fig. 1, this partitioning into CVs is shown for second- and third-order accurate SV cells. Notice that for the third-order cell, the partitioning into CVs is not uniquely defined. This is also true for higher-order SV cells. For the third-order accurate case, the partitioning has one parameter α_3, as illustrated in the figure. Integrating (1) over each CV and applying the Gauss theorem then yields

$$\frac{\mathrm{d}\bar{\mathbf{u}}_{i,j}}{\mathrm{d}t} = -\frac{\mathbf{f}(\mathbf{u}_{i,j+\frac{1}{2}}) - \mathbf{f}(\mathbf{u}_{i,j-\frac{1}{2}})}{x^{\mathrm{b}}_{i,j+\frac{1}{2}} - x^{\mathrm{b}}_{i,j-\frac{1}{2}}} \tag{2}$$

where the $\bar{\mathbf{u}}_{i,j}$ are the averaged conserved variables over the CVs

$$\bar{\mathbf{u}}_{i,j} = \frac{1}{x^{\mathrm{b}}_{i,j+\frac{1}{2}} - x^{\mathrm{b}}_{i,j-\frac{1}{2}}} \int_{x^{\mathrm{b}}_{i,j-\frac{1}{2}}}^{x^{\mathrm{b}}_{i,j+\frac{1}{2}}} \mathbf{u}\,\mathrm{d}x \tag{3}$$

On each cell, the solution can be approximated by a polynomial $\mathbf{U}^{\mathrm{SV}}_i(t,x)$ of degree p

$$\mathbf{u}_i(t,x) \approx \mathbf{U}^{\mathrm{SV}}_i(t,x) \equiv \sum_{j=1}^{p+1} \bar{\mathbf{u}}_{i,j}(t)\bar{L}_{i,j}(x) \tag{4}$$

where the SV basis functions $\bar{L}_{i,j}(x)$ are defined by

$$\frac{1}{x^{\mathrm{b}}_{i,j+\frac{1}{2}} - x^{\mathrm{b}}_{i,j-\frac{1}{2}}} \int_{x^{\mathrm{b}}_{i,j-\frac{1}{2}}}^{x^{\mathrm{b}}_{i,j+\frac{1}{2}}} \bar{L}_{i,k}(x)\mathrm{d}x = \delta_{jk} \tag{5}$$

with δ_{jk} the Kronecker delta function. Using this solution polynomial, the fluxes at the CV-boundaries can be approximated and the right-hand-side of (2) can be evaluated. At the interface between two cells, a Riemann solver $\tilde{\mathbf{F}}^{\mathrm{R,SV}}(\mathbf{u}_{\mathrm{L}}, \mathbf{u}_{\mathrm{R}})$ is used to deal with the discontinuity in the numerical solution. Eq. (2) is then written as

$$\frac{\mathrm{d}\bar{\mathbf{u}}_{i,j}}{\mathrm{d}t} = -\frac{\mathbf{F}^{\mathrm{SV}}_{i,j+\frac{1}{2}} - \mathbf{F}^{\mathrm{SV}}_{i,j-\frac{1}{2}}}{x^{\mathrm{b}}_{i,j+\frac{1}{2}} - x^{\mathrm{b}}_{i,j-\frac{1}{2}}} \tag{6}$$

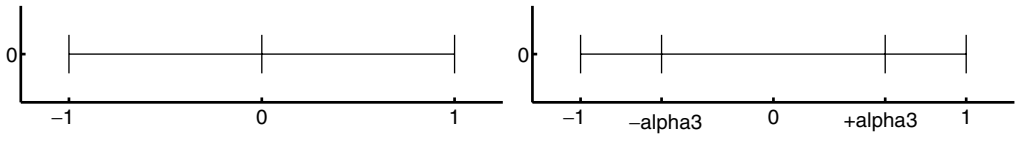

Fig. 1. Second- (left) and third-order (right) accurate 1D SV cells, plotted in a coordinate system local to the cell ($-1 \leqslant \xi \leqslant +1$).

where the $\mathbf{F}^{\mathrm{SV}}_{i,j+\frac{1}{2}}$ are the approximate fluxes. This is a closed system of ordinary differential equations (ODEs) in the SV solution variables $\bar{\mathbf{u}}_{i,j}$, which can be solved in time using any classical algorithm for such systems.

3. Spectral difference method in 1D

The 1D SD method can also be applied to 1D conservation law systems such as (1). The computational domain is again divided in N cells with index i. For a $(p+1)$th-order accurate SD scheme, $p+1$ solution points, with index j, are placed in each cell, at positions $x^{\mathrm{s}}_{i,j}$. The solution variables of the SD method are then the conserved variables $\mathbf{u}_{i,j}$ at these solution points. The solution points support a set of Lagrangian basis polynomials $L_{i,j}(x)$, which allows to approximate the solution with a polynomial $\mathbf{U}^{\mathrm{SD}}_i(t,x)$ of degree p in each cell

$$\mathbf{u}(t,x) \approx \mathbf{U}^{\mathrm{SD}}_i(t,x) \equiv \sum_{j=1}^{p+1} \mathbf{u}_{i,j}(t) L^{\mathrm{s}}_{i,j}(x) \tag{7}$$

The time evolution of the solution variables is governed by (1), evaluated at $x^{\mathrm{s}}_{i,j}$. To compute the derivative of the flux at the solution points, a flux polynomial of degree $p+1$ is introduced. Thus, $p+2$ flux points $x^{\mathrm{f}}_{i,k}$ are placed in each cell i. To ensure a coupling between the cells, two flux points must lie at the cell faces. The distributions of solution and flux points in a second- and a third-order 1D SD cell are plotted in Fig. 2. It can be seen that for the second-order accurate SD cell, the flux points are uniquely defined. For higher-order schemes, the flux point distribution has one or more parameters. For instance, in the third-order case, there is one parameter α_3, as shown in the figure. The solution point distribution is never uniquely defined (except for $p=0$). An approximate value $\mathbf{F}^{\mathrm{SD}}_{i,k}$ of the flux in each of the flux points can then be calculated, using the solution polynomial $\mathbf{U}^{\mathrm{SD}}_i$. For the flux points at the cell boundaries a Riemann solver $\tilde{\mathbf{F}}^{\mathrm{R,SD}}(\mathbf{u}_{\mathrm{L}}, \mathbf{u}_{\mathrm{R}})$ is used to deal with the discontinuity in the numerical solution. Using the fluxes at the flux points, a Lagrangian flux polynomial is then constructed

$$\mathbf{f}(x) \approx \mathbf{F}^{\mathrm{SD}}(x) \equiv \sum_{k=1}^{p+2} \mathbf{F}^{\mathrm{SD}}_{i,k} L^{\mathrm{f}}_{i,k}(x) \tag{8}$$

Finally, the derivative of $\mathbf{F}^{\mathrm{SD}}$ at the solution points can be computed and the following expression is found for the residuals of the SD solution variables:

$$\frac{\mathrm{d}\mathbf{u}_{i,j}}{\mathrm{d}t} = -\left.\frac{\mathrm{d}\mathbf{F}^{\mathrm{SD}}}{\mathrm{d}x}\right|_{i,j} \tag{9}$$

Eq. (9) is a closed system of ODEs in the SD solution variables, which can again be solved in time with a classical algorithm.

4. Equivalence of the SV and SD method in 1D

The following indexes are used throughout this section, for cells, CVs or solution points and CV-boundaries or flux points, respectively:

$$i = 1,\ldots,N; \quad j = 1,\ldots,p+1; \quad k = 1,\ldots,p+2 \tag{10}$$

In 1D, the FV and the FD methods are equivalent for uniform meshes. A similar equivalence exists in 1D for the SV and the SD method.

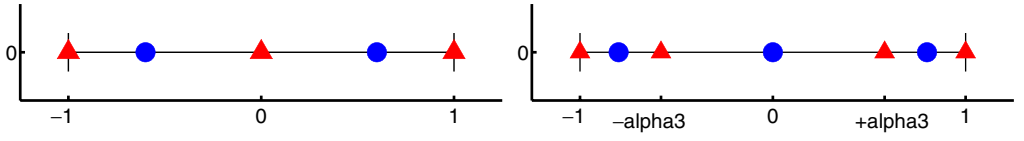

Fig. 2. Second- (left) and third-order (right) accurate 1D SD cells, plotted in a coordinate system local to the cell ($-1 \leqslant \xi \leqslant +1$). Solution (●) and flux (▲) points.

Theorem. *In* $1D$*, a spectral difference method is equivalent to a spectral volume method, and thus* $\mathbf{U}_i^{\mathrm{SV}}(t,x) = \mathbf{U}_i^{\mathrm{SD}}(t,x)$*, provided that*

- *The numerical solution is initialized by locally projecting the exact initial solution on the basis polynomials in each cell*

$$\int_{x_{i-\frac{1}{2}}}^{x_{i+\frac{1}{2}}} \bar{L}_{i,j}(x)\mathbf{U}_i^{\mathrm{SV}}(0,x)\mathrm{d}x = \int_{x_{i-\frac{1}{2}}}^{x_{i+\frac{1}{2}}} \bar{L}_{i,j}(x)\mathbf{u}(0,x)\mathrm{d}x \tag{11}$$

$$\int_{x_{i-\frac{1}{2}}}^{x_{i+\frac{1}{2}}} L_{i,j}^{\mathrm{s}}(x)\mathbf{U}_i^{\mathrm{SD}}(0,x)\mathrm{d}x = \int_{x_{i-\frac{1}{2}}}^{x_{i+\frac{1}{2}}} L_{i,j}^{\mathrm{s}}(x)\mathbf{u}(0,x)\mathrm{d}x \tag{12}$$

- *The CV boundary positions for the SV method are the same as the flux point positions for the SD method*: $x_{i,k-\frac{1}{2}}^{\mathrm{b}} = x_{i,k}^{\mathrm{f}}$.
- *The same Riemann solver is used for both methods*: $\tilde{\mathbf{F}}^{\mathrm{R,SV}} = \tilde{\mathbf{F}}^{\mathrm{R,SD}}$.

Proof. It is sufficient to show that the following two statements are true (∼proof by mathematical induction):

- The initial numerical solution of the SV and the SD method are the same

$$\mathbf{U}_i^{\mathrm{SV}}(0,x) = \mathbf{U}_i^{\mathrm{SD}}(0,x) \tag{13}$$

- If at a certain time t the numerical solutions are the same, then the time derivatives of the numerical solutions are the same as well

$$\mathbf{U}_i^{\mathrm{SV}}(t,x) = \mathbf{U}_i^{\mathrm{SD}}(t,x) \Rightarrow \frac{\partial \mathbf{U}_i^{\mathrm{SV}}}{\partial t} = \frac{\partial \mathbf{U}_i^{\mathrm{SD}}}{\partial t} \tag{14}$$

For the proof for the first statement, consider that both methods use the same solution approximation space (piecewise continuous polynomials of degree p). They only use a different set of basis polynomials. Since the initial numerical solutions are obtained by projecting the initial exact solution on the same solution approximation space, they will be exactly the same: $\mathbf{U}_i^{\mathrm{SV}}(0,x) = \mathbf{U}_i^{\mathrm{SD}}(0,x)$.

The proof for the second statement goes as follows. Since the solution polynomials are identical, the CV-boundaries and the flux points are at the same positions, and the same Riemann solver is used at the cell boundaries, the same flux approximation polynomial can be defined for both methods

$$\mathbf{U}_i^{\mathrm{SV}}(t,x) = \mathbf{U}_i^{\mathrm{SD}}(t,x) \wedge x_{i,k-\frac{1}{2}}^{\mathrm{b}} = x_{i,k}^{\mathrm{f}} \wedge \tilde{\mathbf{F}}^{\mathrm{R,SV}} = \tilde{\mathbf{F}}^{\mathrm{R,SD}} \Rightarrow \mathbf{F}_{i,k-\frac{1}{2}}^{\mathrm{SV}} = \mathbf{F}_{i,k}^{\mathrm{SD}} \Rightarrow \mathbf{F}_i^{\mathrm{SV}}(x) = \mathbf{F}_i^{\mathrm{SD}}(x) \tag{15}$$

In the following, this unique flux polynomial will be referred to as $\mathbf{F}_i$. The average over a CV of the spatial derivative of $\mathbf{F}_i$ is then given by

$$\left.\overline{\frac{\mathrm{d}\mathbf{F}_i}{\mathrm{d}x}}\right|_j = \frac{1}{x_{i,j+\frac{1}{2}}^{\mathrm{b}} - x_{i,j-\frac{1}{2}}^{\mathrm{b}}} \int_{x_{i,j-\frac{1}{2}}^{\mathrm{b}}}^{x_{i,j+\frac{1}{2}}^{\mathrm{b}}} \frac{\mathrm{d}\mathbf{F}_i}{\mathrm{d}x}\mathrm{d}x = \frac{\mathbf{F}_{i,j+\frac{1}{2}}^{\mathrm{SV}} - \mathbf{F}_{i,j-\frac{1}{2}}^{\mathrm{SV}}}{x_{i,j+\frac{1}{2}}^{\mathrm{b}} - x_{i,j-\frac{1}{2}}^{\mathrm{b}}} \tag{16}$$

The following expression is found for the time derivative of the numerical solution, as prescribed by the spectral volume method:

$$\frac{\partial \mathbf{U}_i^{\mathrm{SV}}}{\partial t} = \sum_{j=1}^{p+1} \frac{\mathrm{d}\bar{\mathbf{u}}_{i,j}}{\mathrm{d}t}\bar{L}_{i,j}(x) = -\sum_{j=1}^{p+1} \left(\frac{\mathbf{F}_{i,j+\frac{1}{2}}^{\mathrm{SV}} - \mathbf{F}_{i,j-\frac{1}{2}}^{\mathrm{SV}}}{x_{i,j+\frac{1}{2}}^{\mathrm{b}} - x_{i,j-\frac{1}{2}}^{\mathrm{b}}} \right) \bar{L}_{i,j}(x) \tag{17}$$

and then, using (16)

$$\frac{\partial \mathbf{U}_i^{\mathrm{SV}}}{\partial t} = -\sum_{j=1}^{p+1} \left.\overline{\frac{\mathrm{d}\mathbf{F}_i}{\mathrm{d}x}}\right|_j \bar{L}_{i,j}(x) \equiv -\frac{\mathrm{d}\mathbf{F}_i}{\mathrm{d}x} \tag{18}$$

because $\frac{d\mathbf{F}_i}{dx}$ is a polynomial of the same order as the solution polynomial and is consequently exactly interpolated by the SV basis polynomials $\bar{L}_{i,j}(x)$. Evaluating (18) at the SD solution points yields (9). This shows that the time derivative of the numerical solution as prescribed by the SV method is exactly the same as the one prescribed by the SD method. □

The attentive reader immediately notices that, since no assumptions regarding the SD solution points were made, a consequence of this theorem is that the SD method is independent of the solution point positions. This property will be discussed more elaborately in a future publication.

Notice that the equivalence of the 1D SV and SD methods is not destroyed when a cellwise limiter, such as the total variation diminishing (TVD) or total variation bounded (TVB) limiters that were discussed in [2] (labeled 'SVTVDM' and 'SVTVBM', respectively, therein), is introduced. This immediately follows from the observation that such limiters are based on a condition on the cell means of the solution polynomials, where the solution in a cell is replaced with a limited linear distribution if necessary. Since these solution polynomials are the same for both methods, the equivalence of the SV and SD method is still valid.

The equivalence between SV and SD is not valid in 2D or 3D, since the formulation of both methods then differs fundamentally. For the SD method, the general definition of the residuals associated with the solution variables contains only pointwise operations, to construct a flux polynomial of degree $p+1$ and to compute the derivatives of this polynomial in the solution points. The residuals associated with the SV solution variables are defined in general by integrals of the flux over the CV faces, without constructing a flux polynomial. In 1D however, the CV faces reduce to points, which allows us to draw an analogy with the flux points of the SD method and to conclude that the flux is treated as an identical polynomial of degree $p+1$ by both methods, if the CV faces and the flux points coincide. Notice however that for the SV method, this polynomial is never explicitly constructed or used, since only the values at the CV faces are needed (the SV solution variables are updated using the flux differences at the CV faces, or the net fluxes coming into the CVs). In 2D or 3D, it is not possible to identify such a flux polynomial for the SV method and thus the equivalence fails.

Finally, it should also be noted that the equivalence is no longer valid if a solution approximation space other than the space of piecewise continuous polynomials is used (for instance, the space of piecewise continuous trigonometric functions).

5. Numerical experiments

5.1. 1D linear advection equation

In this section, results obtained for the 1D linear advection equation

$$\frac{\partial u}{\partial t}+\frac{\partial(au)}{\partial x}=0 \tag{19}$$

with $a=1$, are discussed. The computational domain was $0\leqslant x\leqslant 1$, with periodic boundary conditions. The spatial discretization was done with the SV or SD method, always on a uniform mesh. At the cell boundaries, an upwind Riemann flux was used. The initial solution was a Gaussian pulse with a halfwidth equal to 0.05

$$u(0,x)=\exp\left(-\left(\frac{x-0.5}{0.05}\right)^2\right) \tag{20}$$

The numerical solution was initialized by locally projecting this Gaussian pulse on the SV or SD basis functions. For time integration, a third-order TVD Runge–Kutta scheme (see [16]) was used, with a time step Δt small enough to ensure that the error caused by the time marching scheme is negligible compared to that caused by the spatial discretization.

The CV boundary/flux points positions $\xi_k^{b/f}$ of the schemes that were used are included in Table 1, with ξ a local coordinate in each cell, such that $x=0.5(x_{i-\frac{1}{2}}+x_{i+\frac{1}{2}})+0.5(x_{i+\frac{1}{2}}-x_{i-\frac{1}{2}})\xi$. The distributions in this table were determined using an optimization of the wave propagation properties, as described in [15]. For the SD schemes, two different solution point distributions (ξ_j^s) were considered. One solution point distribution is given by

Table 1
CV boundary/flux point positions of the SV/SD schemes that were used

p	$\xi_1^{b/f}$	$\xi_2^{b/f}$	$\xi_3^{b/f}$	$\xi_4^{b/f}$	$\xi_5^{b/f}$	$\xi_6^{b/f}$	$\xi_7^{b/f}$
1	−1.00	0.00	+1.00	–	–	–	–
2	−1.00	−0.58	+0.58	+1.00	–	–	–
3	−1.00	−0.78	0.00	+0.78	+1.00	–	–
4	−1.00	−0.83	−0.36	+0.36	+0.83	+1.00	–
5	−1.00	−0.88	−0.53	0.00	+0.53	+0.88	+1.00

$$\xi_j^s = -\cos\left(\frac{2j-1}{p+1}\pi\right) \quad j = 1,\ldots,p+1 \tag{21}$$

For the second distribution, the solution points are placed at flux points. The only flux point that does not coincide with a solution point is then the one in the middle or just to the left of the middle of the cell.

A grid convergence study of the error at $t = 1.0$ was performed for all these schemes. The same L_1- and L_∞-norm of the error was obtained, up to machine accuracy, for the SV and SD schemes of the same order. These errors are listed in Table 2. Clearly, the expected order of accuracy is achieved in all cases.

5.2. 1D Burger's equation

Results obtained for a nonlinear case, namely for Burger's equation in 1D

$$\frac{\partial u}{\partial t} + \frac{\partial}{\partial x}\left(\frac{u^2}{2}\right) = 0 \tag{22}$$

Table 2
Linear advection of a Gaussian pulse

p	Cell size	#DOF	L_1-error	L_∞-error	L_1-order	L_∞-order
1	0.100000	20	1.38e−1	6.56e−1	–	–
	0.050000	40	7.20e−2	4.92e−1	0.94	0.41
	0.025000	80	4.07e−2	2.89e−1	0.82	0.77
	0.012500	160	1.66e−2	1.58e−1	1.30	0.88
	0.006250	320	4.76e−3	5.15e−2	1.80	1.62
	0.003125	640	1.23e−3	1.33e−2	1.96	1.95
2	0.100000	30	6.26e−2	3.85e−1	–	–
	0.050000	60	2.01e−2	1.48e−1	1.64	1.38
	0.025000	120	2.73e−3	3.09e−2	2.88	2.26
	0.012500	240	1.90e−4	2.66e−3	3.84	3.54
	0.006250	480	1.44e−5	2.02e−4	3.72	3.72
3	0.100000	40	2.33e−2	1.79e−1	–	–
	0.050000	80	3.01e−3	2.61e−2	2.95	2.77
	0.025000	160	1.05e−4	1.57e−3	4.84	4.06
	0.012500	320	4.35e−6	9.84e−5	4.60	4.00
4	0.100000	50	7.27e−3	5.21e−2	–	–
	0.050000	100	5.47e−4	6.18e−3	3.73	3.08
	0.025000	200	2.34e−5	3.33e−4	4.55	4.21
	0.012500	400	8.19e−7	1.13e−5	4.84	4.88
5	0.100000	60	2.33e−3	2.82e−2	–	–
	0.050000	120	6.63e−5	8.70e−4	5.14	5.02
	0.025000	240	1.10e−6	1.79e−5	5.91	5.60
	0.012500	480	1.74e−8	2.66e−7	5.98	6.08

Grid convergence study of the error at $t = 1.0$.

are presented in this section. The computational domain was $-1 \leqslant x \leqslant 1$, with periodic boundary conditions. This domain was discretized with a uniform mesh. The initial solution is a sine function

$$u(0,x) = 1 + \frac{1}{2}\sin(\pi x) \tag{23}$$

which was again imposed using a projection operator. The same third-order TVD R–K scheme was used for time marching, with a sufficiently small time step.

In Table 3, a grid convergence study of the L_1- and L_∞-norms of the error at $t = 0.3$ is listed, for the schemes of Table 1. Again, the same results, up to machine accuracy, were obtained with the SV and SD schemes of the same order. In all cases, the expected order of accuracy is observed.

At $t = 2/\pi$, a shock is formed in the solution. A limiter then has to be introduced to ensure that the monotonicity of the numerical solution is preserved. The numerical solution at $t = 2/\pi$ was computed with the SV and SD schemes, for p ranging from 1 to 5, using both the TVD and TVB cellwise limiters as described in [2]. In all cases, the same numerical solution was obtained with SV and SD, up to machine accuracy. As an example, the solutions obtained using fourth-order ($p = 3$) methods on a mesh with 10 cells are plotted in Fig. 3, along with the exact solution.

Table 3
Nonlinear advection of a sine wave as prescribed by Burger's equation

p	Cell size	#DOF	L_1-error	L_∞-error	L_1-order	L_∞-order
1	0.200000	20	1.16e−2	2.74e−2	–	–
	0.100000	40	3.07e−3	9.97e−3	1.92	1.46
	0.050000	80	7.82e−4	3.09e−3	1.97	1.69
	0.025000	160	1.95e−4	8.11e−4	2.00	1.93
	0.012500	320	4.88e−5	2.08e−4	2.00	1.96
	0.006250	640	1.22e−5	5.24e−5	2.00	1.99
2	0.200000	30	1.35e−3	1.05e−2	–	–
	0.100000	60	1.65e−4	1.75e−3	3.03	2.58
	0.050000	120	2.21e−5	3.60e−4	2.90	2.28
	0.025000	240	2.88e−6	5.59e−5	2.94	2.69
	0.012500	480	3.67e−7	7.74e−6	2.98	2.85
	0.006250	960	4.64e−8	9.98e−7	2.98	2.96
3	0.400000	20	2.51e−3	1.33e−2	–	–
	0.200000	40	7.74e−5	5.60e−4	5.02	4.57
	0.100000	80	1.07e−5	2.18e−4	2.85	1.36
	0.050000	160	5.38e−7	1.39e−5	4.31	3.97
	0.025000	320	3.02e−8	9.25e−7	4.15	3.91
	0.012500	640	1.81e−9	5.86e−8	4.06	3.98
4	0.500000	20	1.85e−3	1.20e−2	–	–
	0.250000	40	5.95e−5	6.95e−4	4.96	4.11
	0.125000	80	3.18e−6	8.09e−5	4.23	2.96
	0.062500	160	8.81e−8	4.00e−6	5.17	4.34
	0.031250	320	3.60e−9	1.61e−7	4.61	4.63
	0.015625	640	1.25e−10	5.77e−9	4.85	4.80
5	0.400000	30	2.47e−4	2.48e−3	–	–
	0.200000	60	3.23e−6	4.99e−5	6.26	5.64
	0.100000	120	1.29e−7	4.70e−6	4.65	3.41
	0.050000	240	1.54e−9	7.56e−8	6.39	5.96
	0.025000	480	2.16e−11	1.34e−9	6.16	5.82

Grid convergence study of the error at $t = 0.3$.

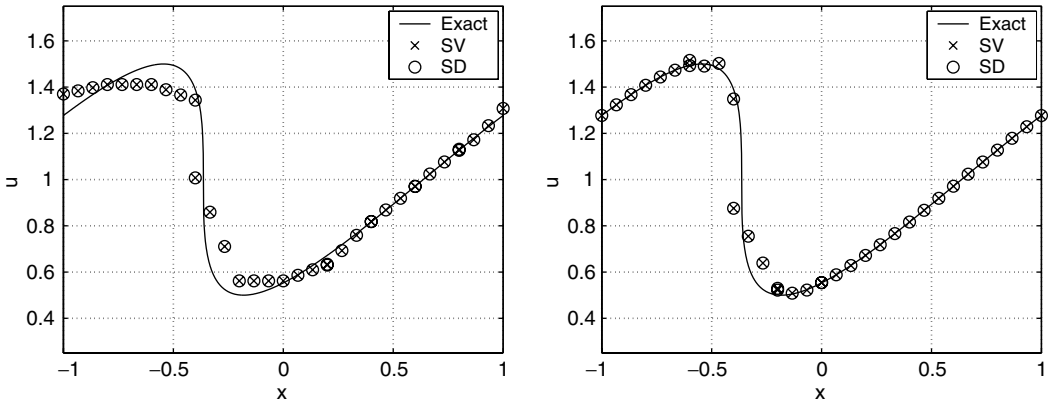

Fig. 3. Solution for Burger's equation at $t = 2/\pi$, on a mesh with 10 cells, obtained with fourth-order SV and SD schemes, combined with a cellwise TVD (left) and a TVB limiter.

6. Conclusions

In this note, the equivalence of the spectral volume and the spectral difference method in 1D was shown. This equivalence was illustrated with the linear advection of a Gaussian pulse and the nonlinear advection of a sine wave, as prescribed by Burger's equation. For both test cases, the same error norms were found with the SV and the SD method, up to machine accuracy. A consequence of this 1D SV–SD equivalence is that the SD method is independent of the solution point positions in 1D. This solution point independence property of the SD method will be reported more elaborately in a future publication.

Acknowledgments

The research presented in this note was done during a stay of the first author at Iowa State University, for which funding was provided by FWO. This funding is gratefully acknowledged.

References

[1] B. Cockburn, C.-W. Shu, TVB Runge–Kutta local projection discontinuous Galerkin finite element method for conservation laws. II: general framework, Mathematics of Computation 52 (1989) 411–435.
[2] Z.J. Wang, Spectral (finite) volume method for conservation laws on unstructured grids: basic formulation, Journal of Computational Physics 178 (2002) 210–251.
[3] Z.J. Wang, Y. Liu, Spectral (finite) volume method for conservation laws on unstructured grids. II: extension to two-dimensional scalar equation, Journal of Computational Physics 179 (2002) 665–697.
[4] Z.J. Wang, Y. Liu, Spectral (finite) volume method for conservation laws on unstructured grids. III: one dimensional systems and partition optimization, Journal of Scientific Computing 20 (2004) 137–157.
[5] Z.J. Wang, L. Zhang, Y. Liu, Spectral (finite) volume method for conservation laws on unstructured grids. IV: extension to two-dimensional Euler equations, Journal of Computational Physics 194 (2) (2004) 716–741.
[6] Y. Liu, M. Vinokur, Z.J. Wang, Spectral (finite) volume method for conservation laws on unstructured grids. V: extension to three-dimensional systems, Journal of Computational Physics 212 (2006) 454–472.
[7] Y. Sun, Z.J. Wang, Y. Liu, Spectral (finite) volume method for conservation laws on unstructured grids. VI: extension to viscous flow, Journal of Computational Physics 215 (2006) 41–58.
[8] Z.J. Wang, Y. Liu, Extension of the spectral volume method to high-order boundary representation, Journal of Computational Physics 211 (2006) 154–178.
[9] Yen Liu, Marcel Vinokur, Z.J. Wang, Spectral difference method for unstructured grids. I: basic formulation, Journal of Computational Physics 216 (2006) 780–801.
[10] Z.J. Wang, Yen Liu, Georg May, Antony Jameson, Spectral difference method for unstructured grids. II: extension to the Euler equations, Journal of Scientific Computing (2006), doi:10.1007/s10915-006-9113-9.
[11] D.A. Kopriva, A conservative staggered-grid Chebyshev multidomain method for compressible flows. II: semi-structured method, Journal of Computational Physics 128 (1996) 475.
[12] Q.-Y. Chen, Partitions of a simplex leading to accurate spectral (finite) volume reconstruction, SIAM Journal on Scientific Computing 27 (4) (2006) 1458–1470.

[13] Q.-Y. Chen, Partitions for spectral (finite) volume reconstruction in the tetrahedron, IMA Preprint Series # 2035, April 2005.
[14] K. Van den Abeele, T. Broeckhoven, C. Lacor, Dispersion and dissipation properties of the 1D spectral volume method and application to a *p*-multigrid algorithm, Journal of Computational Physics 224 (2) (2007) 616–636.
[15] K. Van den Abeele, C. Lacor, An accuracy and stability study of the 2D spectral volume method, Journal of Computational Physics 226 (1) (2007) 1007–1026.
[16] C.-W. Shu, Total variation diminishing Runge–Kutta schemes, SIAM Journal of Scientific and Statistical Computing 9 (1988) 1073–1084.